


Singlet fermion dark matter and Dirac neutrinos from Peccei-Quinn symmetry

Cristian D. R. Carvajal*

*Instituto de Física, Universidad de Antioquia, Calle 70 No. 52-21, Medellín, Colombia
and Instituto Tecnológico Metropolitano, Facultad de Ciencias, Medellín, Colombia.*

Robinson Longas[†], Oscar Rodríguez,[‡] and Óscar Zapata[§]

Instituto de Física, Universidad de Antioquia, Calle 70 No. 52-21, Medellín, Colombia.

 (Received 4 November 2021; accepted 17 December 2021; published 4 January 2022)

The Peccei-Quinn (PQ) mechanism not only acts as an explanation for the absence of strong charge parity (CP) violation but also can play a main role in the solution to other open questions in particle physics and cosmology. Here we consider a model that identifies the PQ symmetry as a common thread in the solution to the strong CP problem, the generation of radiative Dirac neutrino masses and the origin of a multicomponent dark sector. Specifically, scotogenic neutrino masses arise at one-loop level with the lightest fermionic mediator field acting as the second dark matter (DM) candidate thanks to the residual Z_2 symmetry resulting from the PQ symmetry breaking. We perform a phenomenological analysis addressing the constraints coming from the direct searches of DM, neutrino oscillation data and charged lepton flavor violating (LFV) processes. We find that the model can be partially probed in future facilities searching for weakly interacting massive particles and axions, and accommodates rates for rare leptonic decays that are within the expected sensitivity of upcoming LFV experiments.

DOI: [10.1103/PhysRevD.105.015003](https://doi.org/10.1103/PhysRevD.105.015003)

I. INTRODUCTION

The apparent nonobservation of CP violation in the QCD Lagrangian represents one of the most active subjects in high-energy physics, both theoretical and experimentally speaking. In the theory side, the absence of strong CP violation can be dynamically explained invoking the Peccei-Quinn (PQ) mechanism [1], which considers the spontaneous breaking of an anomalous global $U(1)$ symmetry with the associated pseudo-Nambu-Goldstone boson, the (QCD) axion [2,3]. The axion itself turns to be a promising candidate for making up the dark matter (DM) of the Universe thanks to a variety of production mechanisms [4], for instance via the vacuum misalignment mechanism [5–7]. Besides this, it is remarkable that the physics behind the PQ mechanism can be also used to address other open questions in particle physics and

cosmology such as neutrino masses [8–15], baryon asymmetry [16–19] and inflation [20–23].

The recent analysis [24] considering the PQ mechanism as being responsible for the massiveness of neutrinos revealed that it is also possible to consistently accommodate radiative Dirac neutrino masses¹ with a viable weakly interacting massive particle (WIMP) DM candidate, thus providing a set of multicomponent scotogenic models with Dirac neutrinos. Concretely, in these scenarios one-loop Dirac neutrino masses are generated through the $d = 5$ effective operator $\bar{L} \tilde{H} N_R S$ [40,41] once the axionic field S develops a vacuum expectation value, with the contributions arising from the tree-level realizations of such an operator being forbidden thanks to the charge assignment. As a further consequence of the PQ symmetry, the residual discrete symmetry that is left over renders stable the lightest particle mediating the neutrino masses, and since such a particle must be electrically neutral, it turns out that the setup also accommodates a second DM species [26,29,42–45].

In this work we perform a phenomenological analysis of the T3-1-A-I model introduced in Ref. [24]. In order to determine the viable parameter space of the model we take into account the constraints coming from direct detection

*cdavid.ruiz@udea.edu.co; cristianruiz6246@correo.itm.edu.co

†robinson.longas@udea.edu.co

‡oscar.rodriiguez@udea.edu.co

§oalberto.zapata@udea.edu.co

Published by the American Physical Society under the terms of the Creative Commons Attribution 4.0 International license. Further distribution of this work must maintain attribution to the author(s) and the published article's title, journal citation, and DOI. Funded by SCOAP³.

¹See Refs. [25–39] for recent and related works.

experiments, lepton flavor violation (LFV) processes, DM relic density, and neutrino physics. We find that for a wide and typical range of the parameter values, the model easily satisfies these constraints and, additionally, future experiments will be able to test a considerable portion of the parameter space.

The layout of this paper is organized as follows. The main features of the model are presented in Sec. II. In Sec. III we determine the elastic-scattering cross section between the WIMP particle and nucleons, and estimate the expected number of events in current and future direct detection experiments. Sec. IV is dedicated to a numerical analysis addressing the DM and LFV phenomenology. Finally, we conclude in Sec. V.

II. THE MODEL

As usual, in models with massive Dirac neutrinos, this model extends the Standard Model (SM) with three singlet Weyl fermions $N_{R\beta}$ ($\beta = 1, 2, 3$)—the right-handed partners of the SM neutrinos. The one-loop neutrino mass generation additionally demands [24] the introduction of one $SU(2)_L$ doublet scalar H_2 , one singlet scalar Φ , and two singlet Dirac fermions ψ_i ($i = 1, 2$). As the last piece we have a chiral exotic down-type quark D which is added in order to realize the hadronic Kim-Shifman-Vainshtein-Zakharov (KSVZ)-type axion model [46,47]. In Table I the charge assignments under the $U(1)_L$ and $U(1)_{PQ}$ global symmetries are displayed, as well as under the remnant Z_2 symmetry. Notice that under this discrete symmetry the mediator fields in the neutrino mass diagram are odd, which implies that the lightest of them can be considered as a (WIMP-like) DM candidate.²

The relevant part of the scalar potential can be expressed as

$$\begin{aligned} \mathcal{V} \supset & -\mu_1^2 |H_1|^2 + \lambda_1 |H_1|^4 + \mu_S^2 |S|^2 + \lambda_S |S|^4 + \mu_2^2 |H_2|^2 \\ & + \lambda_2 |H_2|^4 + \lambda_3 |H_1|^2 |H_2|^2 + \lambda_4 |H_1^\dagger H_2|^2 \\ & + \mu_\Phi^2 |\Phi|^2 + \lambda_\Phi |\Phi|^4 + \lambda_{h\Phi} |H_1|^2 |\Phi|^2 \\ & + \lambda' (\Phi^* S \tilde{H}_2^\dagger \tilde{H}_1 + \text{H.c.}), \end{aligned} \quad (1)$$

where the coupling constants associated to the quartic-interaction terms $|\Phi|^2 |S|^2$, $|H_2|^2 |S|^2$, $|H_2|^2 |\Phi|^2$, and $|H_1|^2 |S|^2$ have been assumed to be small. Since the $(H_1^\dagger H_2)^2 + (H_2^\dagger H_1)^2$ term is forbidden, it follows that the neutral component of H_2 remains as a complex field and does not get split into a CP -even and a CP -odd field. Nevertheless, it does get mixed with Φ through the term proportional to λ' (since both scalar fields do not acquire a nonzero vacuum expectation value). We parametrize the scalar fields as

²We assume that the lightest particle charged under the PQ symmetry is electrically neutral.

TABLE I. Lepton number and PQ charge assignments for the model particles. Here, both the SM Higgs, H_1 , and the ordinary quarks are even under the discrete symmetry and neutral under the global ones. The transformation properties under the remnant Z_2 symmetry are also shown. β is a family index ($\beta = 1, 2, 3$) and $i = 1, 2$.

	L_β	$\ell_{R\beta}$	$N_{R\beta}$	S	ψ_i	Φ	H_2	D_L	D_R
$U(1)_L$	1	1	1	0	1	0	0	0	0
$U(1)_{PQ}$	2	2	0	2	3	3	1	1	-1
Z_2	+	+	+	+	-	-	-	-	-

$$S = \frac{1}{\sqrt{2}}(\rho + v_S)e^{ia/v_S}, \quad H_1 = \begin{pmatrix} 0 \\ \frac{v_{SM}+h}{\sqrt{2}} \end{pmatrix}, \quad H_2 = \begin{pmatrix} H^+ \\ H^0 \end{pmatrix}, \quad (2)$$

where ρ stands for the radial component of the field S whose mass is set by the scale of the PQ symmetry breaking v_S , whereas the angular part of S corresponds to the QCD axion a , h is the SM Higgs boson, and $v_{SM} = 246.22$ GeV.

In the basis (H^0, Φ) , the mass matrix for the Z_2 -odd neutral scalars

$$\mathcal{M}_0 = \begin{pmatrix} \mu_2^2 + \frac{1}{2}(\lambda_3 + \lambda_4)v_{SM}^2 & \frac{1}{2}\lambda'v_Sv_{SM} \\ \frac{1}{2}\lambda'v_Sv_{SM} & \mu_\Phi^2 + \frac{1}{2}\lambda_{h\Phi}v_{SM}^2 \end{pmatrix}, \quad (3)$$

leads to the mass eigenstates $S_{1,2}$ (both with two degrees of freedom since they are complex) via the transformation

$$H^0 = \cos \varphi S_1 + \sin \varphi S_2 = \sum_{j=1,2} C_{Hj} S_j \equiv C_{Hj} S_j, \quad (4)$$

$$\Phi = -\sin \varphi S_1 + \cos \varphi S_2 = \sum_{j=1,2} C_{\Phi j} S_j \equiv C_{\Phi j} S_j, \quad (5)$$

where we have defined $C_{H1} = \cos \varphi$, $C_{H2} = \sin \varphi$, $C_{\Phi 1} = -\sin \varphi$, and $C_{\Phi 2} = \cos \varphi$. The mixing angle is defined through the expression³

$$\sin(2\varphi) = \frac{\lambda'v_{SM}v_S}{m_{S_2}^2 - m_{S_1}^2}, \quad (6)$$

with $m_{S_{1,2}}$ being the eigenvalues of \mathcal{M}_0 . In our analysis we will take $m_{S_1} < m_{S_2}$, which implies that for $\varphi \rightarrow 0$ the heavier scalar is mainly singlet, whereas for $\varphi \rightarrow \pm\pi/2$ the heavier one is mainly doublet. For the charged scalar H^\pm

³A tiny value for λ' is not only necessary to reproduce the observed neutrino phenomenology but also to have the complex scalars $S_{1,2}$ at or below the TeV mass scale. This is in consonance with the requirement of demanding a tiny value for the scalar couplings between the axion field S and the other scalar fields, as happens in most of the axion models.

we find that its mass is given by $m_{H^\pm}^2 = \mu_2^2 + \frac{1}{2}\lambda_3 v_{\text{SM}}^2$, just as happens in the inert doublet model.

A. Neutrino masses and charged LFV

The new Yukawa interactions involving the SM leptons are given by

$$\mathcal{L}_Y = y_{i\beta}\bar{\psi}_i\tilde{H}_2^\dagger L_\beta + h_{\beta i}\Phi^*\bar{N}_{R\beta}\psi_i + \text{H.c.}, \quad (7)$$

where $y_{i\beta}$ and $h_{\beta i}$ are 2×3 and 3×2 Yukawa matrices, respectively. After the spontaneous symmetry breaking, scotogenic Dirac neutrino masses are generated at one loop [40,41,48–57] as is illustrated in Fig. 1. The effective mass matrix can be written as

$$(M_\nu)_{\alpha\beta} = \sum_i h_{\alpha i} y_{i\beta} \kappa_i, \quad (8)$$

where

$$\kappa_i = \frac{\sin(2\varphi)}{32\pi^2} m_{\psi_i} \left[F\left(\frac{m_{S_2}^2}{m_{\psi_i}^2}\right) - F\left(\frac{m_{S_1}^2}{m_{\psi_i}^2}\right) \right], \quad (9)$$

and $F(x) = x \ln(x)/(x-1)$. The Dirac neutrino mass matrix M_ν can be diagonalized through $M_\nu = VM_\nu^{\text{diag}}U^\dagger$, where U and V are unitary matrices and M_ν^{diag} is a diagonal mass matrix containing, in general, three mass eigenvalues different from zero. However, due to the flavor structure of M_ν only two neutrinos are massive [$\det(M_\nu) = 0$]. In the basis where the charged lepton mass matrix is diagonal the U unitary matrix can be identified with the Pontecorvo-Maki-Nakagawa-Sakata (PMNS) matrix [58], whereas V can be assumed diagonal without loss of generality. This allows us to express the y -Yukawa couplings in terms of the h ones. In the case of the normal neutrino mass hierarchy (NH)

$$\begin{aligned} y_{1\beta} &= \frac{h_{32}m_2U_{\beta 2}^* - h_{22}m_3U_{\beta 3}^*}{(h_{21}h_{32} - h_{31}h_{22})k_1}, \\ y_{2\beta} &= \frac{h_{21}m_3U_{\beta 3}^* - h_{31}m_2U_{\beta 2}^*}{(h_{21}h_{32} - h_{31}h_{22})k_2}, \end{aligned} \quad (10)$$

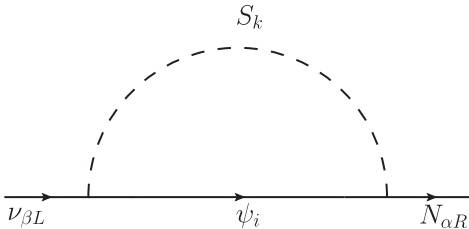


FIG. 1. One-loop Feynman diagram leading to Dirac neutrino masses. The loop mediators are the singlet fermions $\psi_{1,2}$ and the neutral scalars $S_{1,2}$.

with $h_{11} = h_{12} = 0$, whereas in the inverted hierarchy (IH) case

$$\begin{aligned} y_{1\beta} &= \frac{h_{12}m_2U_{\beta 2}^* - h_{22}m_3U_{\beta 1}^*}{(h_{12}h_{21} - h_{11}h_{22})k_1}, \\ y_{2\beta} &= \frac{h_{21}m_3U_{\beta 1}^* - h_{11}m_2U_{\beta 2}^*}{(h_{12}h_{21} - h_{11}h_{22})k_2}, \end{aligned} \quad (11)$$

with $h_{31} = h_{32} = 0$. Notice that one of the right-handed neutrinos becomes decoupled because we are considering a scenario with the minimal set of singlet fermions.⁴

Although Diracness of neutrino masses is compatible with the conservation of the total lepton number, family lepton number violation is unavoidable due to neutrino oscillations. In this model, LFV processes involving charged leptons such as $\ell_\alpha \rightarrow \ell_\beta \gamma$, $\ell_\alpha \rightarrow 3\ell_\beta$, and $\mu - e$ conversion in nuclei are induced at one-loop level, involving only $y_{i\beta}$ Yukawa interactions and mediated by the H^\pm charged scalar and the ψ_i neutral fermions. The decay rate for the $\ell_\alpha \rightarrow \ell_\beta \gamma$ processes (see the top left panel of Fig. 2) neglecting the lepton masses at the final states is given by

$$\begin{aligned} \Gamma(\ell_\alpha \rightarrow \ell_\beta \gamma) &= \frac{e^2 m_\alpha^5}{16^3 \pi^5 m_{H^\pm}^4} \sum_i |y_{i\alpha} y_{i\beta}^*|^2 \\ &\times \left[\frac{2t_i^2 + 5t_i - 1}{12(t_i - 1)^3} - \frac{t_i^2 \log t_i}{2(t_i - 1)^4} \right]^2, \end{aligned} \quad (12)$$

where $t_i \equiv m_{\psi_i}^2/m_{H^\pm}^2$. Concerning the $\ell_\alpha \rightarrow \ell_\beta \bar{\ell}_\beta \ell_\beta$ processes, there are two kinds of diagrams (see Fig. 2); the γ - and Z -penguin diagrams (top-right panel) and the box diagrams (bottom panel). The contribution from the Higgs-penguin diagrams is suppressed for the first two charged lepton generations due to their small Yukawa couplings.⁵ It follows that the $\ell_\alpha \rightarrow \ell_\beta \bar{\ell}_\beta \ell_\beta$ processes contain four kind of contributions: the photonic monopole, photonic dipole, Z -penguin, and box diagrams.⁶ In contrast, the photonic dipole contribution is the only one present in the $\ell_\alpha \rightarrow \ell_\beta \gamma$ processes. Finally, the $\mu - e$ conversion diagrams are obtained when the pair of lepton lines attached to

⁴In the scenario with three singlet fermions, all the neutrino eigenstates would be massive.

⁵The contribution of those processes involving tau leptons is not negligible, but the corresponding limits are less restrictive.

⁶Notice that the Yukawa interactions also lead to neutrino three-body decays $\nu_h \rightarrow \nu_i \bar{\nu}_i \nu_l$, with $m_{\nu_h} > m_{\nu_l}$, via a box diagram similar to the bottom panel in Fig. 2, with the charged leptons replaced by neutrinos and the charged scalar H^\pm by the neutral one H^0 . Since the decay rate for these processes [59] is proportional to the ratio $m_{\nu_h}^5/m_{S_1}^4$, the expected lifetime is several orders of magnitude larger than the age of the Universe.

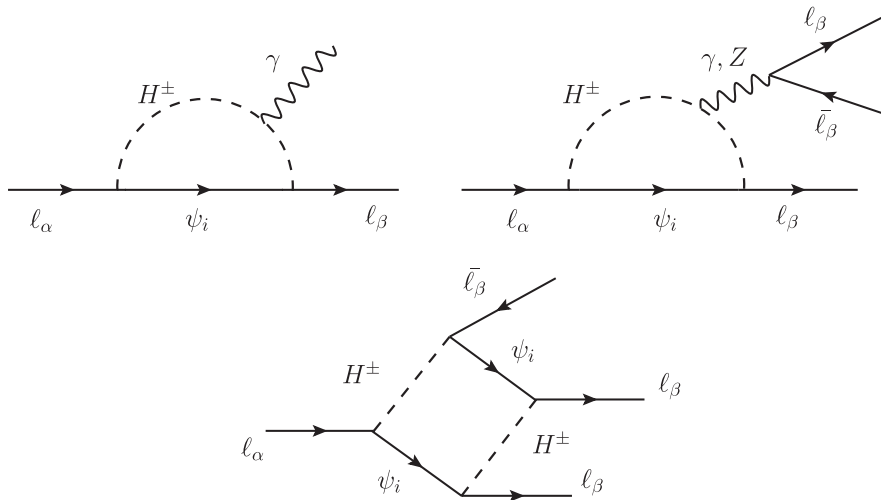


FIG. 2. Feynman diagrams for the $\ell_\alpha \rightarrow \ell_\beta \gamma$ and $\ell_\alpha \rightarrow \ell_\beta \bar{\ell}_\beta \ell_\beta$ charged LFV processes present in the model.

the photon and Z boson in the penguin diagrams (see top panels of Fig. 2) are replaced by a pair of light quark lines.⁷ For the $\mu - e$ conversion in nuclei there are no box diagrams since the Z_2 -odd particles do not couple to quarks at tree level. Accordingly, the photonic nondipole and dipole terms along with the Z-penguin one are the only terms that contribute to the $\mu - e$ conversion processes. In this work we calculate the rates for $\ell_\alpha \rightarrow \ell_\beta \bar{\ell}_\beta \ell_\beta$ and $\mu - e$ through the chain SARAH [60,61], SPheno [62,63], and FlavorKit [64].

B. Two-component dark matter

The natural DM candidate in models featuring a PQ symmetry is the axion itself since the associated energy density decreases as nonrelativistic matter does [4,65–67]. The amount of axion relic abundance depends on whether the PQ symmetry is broken before or after inflation. On the one hand, if PQ symmetry is broken after the inflationary epoch, the axion field would be randomly distributed over the whole range $(0, 2\pi v_S)$, meaning that the initial misalignment angle θ_a takes different values in different patches of the Universe resulting in the average $\langle \theta_a \rangle = \pi/\sqrt{3}$. In this case, topological defects such as string axions and domain walls [68–71] also contribute to the axion relic abundance. On the other hand, when PQ symmetry is broken before the inflationary epoch and is not restored during the reheating phase the axion field is uniform over the observable Universe, meaning that the initial misalignment angle takes a single value in the interval $(0, 2\pi]$.

For simplicity purposes, we assume that the reheating temperature after inflation is below the PQ symmetry-breaking scale, in which case the axion abundance is settled to [6,72]

⁷Higgs-penguin diagrams are again suppressed, in this case by the Yukawa couplings to light quarks.

$$\Omega_a h^2 \approx 0.18 \theta_a^2 \left(\frac{v_S}{10^{12} \text{ GeV}} \right)^{1.19}. \quad (13)$$

It follows that the axion can be the main DM constituent if $v_S \sim 10^{12}$ GeV for a nonfine-tuned θ_a [that is $\theta_a \approx \mathcal{O}(1)$]. Under this premise, the axion window becomes $m_a \sim (1 - 10) \mu\text{eV}$. Nevertheless, the axion can give a subdominant contribution to the relic DM abundance for lower values of v_S , thus allowing for a multicomponent DM scenario.

In addition to the axion, this model brings along with a second DM candidate since the remnant Z_2 symmetry renders stable the lightest particle charged under it. The case of S_1 being that candidate is ruled out since direct-detection searches have excluded models where the DM candidate has a direct coupling to the Z gauge boson. Therefore, $\psi_1 \equiv \psi$ becomes the second viable DM candidate of the model. According to Eq. (7), ψ only interacts with the SM particles via the Yukawa interactions y and h , and since these must be non-negligible in order to explain the neutrino oscillation parameters, ψ necessarily reaches thermal equilibrium with the SM plasma. The ψ relic abundance is determined by the cross sections of the annihilation and coannihilation processes $\bar{\psi}\psi \rightarrow \bar{\ell}\ell, \bar{\nu}\nu$ and $H^+\psi \rightarrow \ell\gamma$, respectively. Let us stress that the h interactions can actually take large values because they are not part of the LFV processes, which means that ψ may feature a large annihilation cross section. If the fermion DM and scalar-mediator masses are assumed to be sufficiently nondegenerate, coannihilations can be neglected, and thus the relic abundance simply depends on the ψ -annihilation cross section. In our numerical analysis, nonetheless, we use micrOMEGAS [73] in order to take into account all the relevant processes that contribute to the setting of the relic abundance of ψ .

III. DIRECT DETECTION OF FERMION DARK MATTER

Being a SM singlet that couples to leptons and Z_2 -odd scalars, ψ does not have tree-level interactions with the SM quarks. However, the interactions involving Z_2 -odd particles allow us to construct effective interactions at one-loop level between a singlet fermion DM and quarks.

In the basis of mass eigenstates, the relevant interaction terms involved in the direct detection of ψ are

$$-\mathcal{L} \supset C_{\psi S\nu}^{\beta i} \bar{\psi}_R S_i \nu_{\beta L} + C_{\psi H e}^{\beta} \bar{\psi}_R H^{\pm} e_{\beta L} + C_{\psi S N}^{\beta i} \bar{\psi}_L S_i N_{\beta R} + C_{SSh}^{ij} S_i^* S_j h + \text{H.c.}, \quad (14)$$

where a sum over repeated Latin and Greek indices is implied. The new coefficients in this expression are defined as

$$C_{\psi S\nu}^{\beta i} = y_{1\beta} C_{Hi}, \quad C_{\psi H e}^{\beta} = -y_{1\beta}, \quad C_{\psi S N}^{\beta i} = h_{\beta 1} C_{\Phi i},$$

$$C_{SSh}^{ij} = \lambda_{h\Phi} v_H C_{\Phi i} C_{\Phi j} + \frac{\lambda' v_S}{2} C_{\Phi i} C_{Hj}. \quad (15)$$

The interplay of the above interactions with the gauge and scalar interactions lead to the effective one-loop couplings between ψ and the Higgs photon, and Z bosons as shown in Fig. 3.

The differential spin-independent cross section for the fermion DM particle being scattered by a target nucleus of mass m_T and atomic and mass numbers A and Z can be expressed as [74]

$$\frac{d\sigma_{\psi T}}{dE_R} = F_c^2(E_R) \left\{ \frac{Z^2 e^2}{4\pi} \left[\frac{1}{E_R} - \frac{1}{E_R^{\max}(v_{\text{rel}}^2)} \right] (C_M^{\gamma})^2 + \frac{Z^2 e^2}{4\pi v_{\text{rel}}^2} \frac{1}{E_R} (C_E^{\gamma})^2 + \frac{m_T}{2\pi v_{\text{rel}}^2} \left| Z \left(f_S^p + f_V^p - e C_R^{\gamma} - \frac{e}{2m_{\psi}} C_M^{\gamma} \right) + (A - Z)(f_S^n + f_V^n) \right|^2 \right\}. \quad (16)$$

Here, v_{rel} is the relative velocity between ψ and the nucleus, and E_R denotes the recoil energy of the nucleus due to the interaction. The maximum value of E_R , E_R^{\max} , is related to v_{rel} through

$$E_R^{\max}(v_{\text{rel}}^2) = \frac{2m_{\psi}^2 m_T v_{\text{rel}}^2}{(m_{\psi} + m_T)^2}. \quad (17)$$

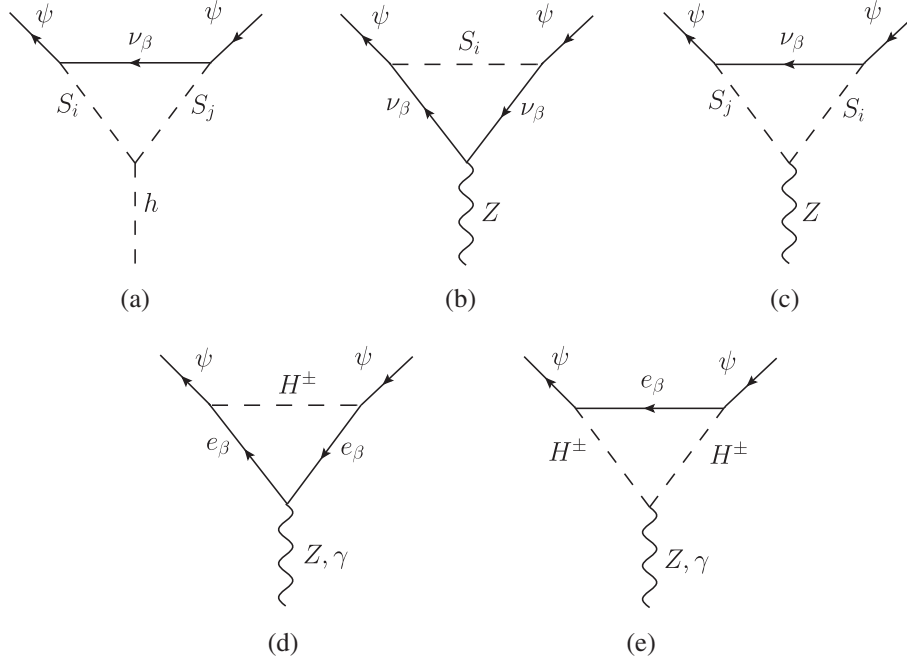


FIG. 3. One-loop effective couplings between the fermion DM candidate and the SM neutral bosons.

The effective couplings $C_{M(E)}^\gamma$ and C_R^γ correspond to the Wilson coefficients describing the interaction with the photon field as a result of the magnetic (electric) dipole moment and the charge radius of the fermion DM. In this model these quantities are given by

$$C_M^\gamma = -\frac{e}{2(4\pi)^2 m_\psi} |y_{1\beta}|^2 g_{M1}(m_\psi, m_{H^\pm}, m_{e_\beta}), \quad (18)$$

$$C_E^\gamma = 0, \quad (19)$$

$$C_R^\gamma = -\frac{e}{2(4\pi)^2 m_\psi^2} |y_{1\beta}|^2 g_{R1}(m_\psi, m_{H^\pm}, m_{e_\beta}), \quad (20)$$

where explicit expressions for the one-loop functions g_{M1} and g_{R1} are reported in the Appendix. The vanishing of C_E^γ has its origin in the absence of a coupling between the right-handed electron and ψ as can be seen from Eq. (14). The interaction with nucleons is described by the effective scalar and vector couplings $f_S^{(N)}$ and $f_V^{(N)}$ ($N = p, n$), respectively. The scalar coupling is given in terms of the ψ -quark (-gluon) scalar couplings $C_S^{q(g)}$ and the matrix elements $f_{T_q}^{(N)} = \langle N | m_q \bar{q} q | N \rangle / m_N$ ⁸. From Ref. [76] it reads

$$f_S^{(N)} = m_N \left[\sum_{q=u,d,s} C_S^q f_{T_q}^{(N)} - \frac{8}{9} C_S^g f_{T_G}^{(N)} \right], \quad (21)$$

where m_N is the nucleon mass. On the other hand, the vector coupling can be expressed in terms of the ψ -quark vector couplings C_V^q as

$$f_V^{(N)} = \begin{cases} 2C_V^u + C_V^d, & \text{for } N = p, \\ C_V^u + 2C_V^d, & \text{for } N = n. \end{cases} \quad (22)$$

In this model, the ψ effective interactions with quarks and gluons can be cast as

$$C_S^q = -4C_S^g = -\frac{1}{\sqrt{2}m_h^2 v_{\text{SM}}} C_{\psi h}, \quad (23)$$

$$C_V^u = -\frac{2}{v_{\text{SM}}^2} \left(\frac{1}{2} - \frac{4}{3} \sin^2 \theta_W \right) C_{\psi Z}, \quad (24)$$

$$C_V^d = -\frac{2}{v_{\text{SM}}^2} \left(-\frac{1}{2} + \frac{2}{3} \sin^2 \theta_W \right) C_{\psi Z}, \quad (25)$$

being $C_{\psi h(Z)}$ the effective scalar (vector) coupling between ψ and the Higgs (Z) boson. These are given by

$$C_{\psi h} = \frac{\tilde{g}_{h1}(m_\psi, m_{S_i}, m_{S_j}, m_{\nu_\beta})}{\sqrt{2}(4\pi)^2 m_\psi} C_{\Phi i} \left(\lambda_{h\Phi} v_{\text{SM}} C_{\Phi j} + \frac{\lambda' v_S}{2} C_{Hj} \right) (|y_{1\beta}|^2 C_{Hi} C_{Hj} + |h_{\beta 1}|^2 C_{\Phi i} C_{\Phi j}), \quad (26)$$

$$\begin{aligned} C_{\psi Z} = & \frac{|y_{1\beta}|^2}{2(4\pi)^2} \left\{ \left(\sin^2 \theta_W - \frac{1}{2} \right) [g_{Z1}(m_\psi, m_{H^\pm}, m_{e_\beta}, m_{e_\beta}) + \tilde{g}_{Z1}(m_\psi, m_{H^\pm}, m_{H^\pm}, m_{e_\beta})] \right. \\ & + \sin^2 \theta_W \frac{m_{e_\beta}^2}{m_\psi^2} g_{Z2}(m_\psi, m_{H^\pm}, m_{e_\beta}, m_{e_\beta}) + \frac{C_{Hi}^2}{2} [g_{Z1}(m_\psi, m_{S_i}, m_{\nu_\beta}, m_{\nu_\beta}) \\ & \left. + C_{Hj}^2 \tilde{g}_{Z1}(m_\psi, m_{S_i}, m_{S_j}, m_{\nu_\beta})] \right\} + \frac{|h_{\beta 1}|^2}{2(4\pi)^2} \frac{C_{Hi} C_{\Phi i} C_{Hj} C_{\Phi j}}{2} \tilde{g}_{Z1}(m_\psi, m_{S_i}, m_{S_j}, m_{\nu_\beta}). \end{aligned} \quad (27)$$

⁸For the numerical analysis shown in Sec. IV we considered the values

$$\begin{aligned} f_{T_u}^{(p)} &= 0.018, & f_{T_d}^{(p)} &= 0.027, & f_{T_s}^{(p)} &= 0.037, \\ f_{T_G}^{(p)} &= 1 - \sum_{q=u,d,s} f_{T_q}^{(p)} = 0.918, \\ f_{T_u}^{(n)} &= 0.013, & f_{T_d}^{(n)} &= 0.040, & f_{T_s}^{(n)} &= 0.037, \\ f_{T_G}^{(n)} &= 1 - \sum_{q=u,d,s} f_{T_q}^{(n)} = 0.090, \end{aligned}$$

as suggested by [75].

As indicated above, a sum over repeated indices is implied and the definitions of the one-loop functions \tilde{g}_{h1} , g_{Z1} , \tilde{g}_{Z1} , and g_{Z2} are reported in Appendix. The recoil-energy dependent nuclear form factor $F_c^2(E_R)$ in Eq. (16) reads [77,78]

$$F_c^2(E_R) = \left[3 \frac{j_1(qR)}{qR} \right]^2 e^{-q^2 s^2}, \quad (28)$$

where j_1 is the spherical Bessel function of the first kind, $q = \sqrt{2m_T E_R}$ and $R = \sqrt{c^2 + \frac{7}{3}\pi^2 a^2 - 5s^2}$ with $c = (1.23A^{1/3} - 0.6)$ fm, $a = 0.52$ fm and $s = 0.9$ fm.

In order to estimate the expected number of ψ -nuclei scattering events in a direct detection experiment like XENON1T [79], we calculate the differential event rate per unit of detector mass through [74]

$$\frac{dR}{dE_R} = \frac{\rho_{\text{DM}}}{m_T m_\psi} \int_{v_{\min}(E_R)}^{\infty} d^3 \mathbf{v}_{\text{rel}} v_{\text{rel}} f_{\oplus}(\mathbf{v}_{\text{rel}}) \frac{d\sigma_{\psi T}}{dE_R}. \quad (29)$$

Here $\rho_{\text{DM}} \approx 0.3 \text{ GeV/cm}^3$ is the local DM density, $v_{\min}(E_R)$ is the minimum speed needed to yield a recoil with energy E_R , which can be determined from

$$v_{\min}(E_R) = \sqrt{\frac{(m_\psi + m_T)^2 E_R}{2m_\psi m_T}}, \quad (30)$$

and $f_{\oplus}(\mathbf{v}_{\text{rel}})$ stands for the DM velocity distribution measured with respect to the lab frame. With respect to the galactic frame, this distribution is assumed to follow a Maxwell-Boltzmann one, i.e.,

$$f(\mathbf{v}) = \begin{cases} \frac{1}{N} e^{-|\mathbf{v}|^2/v_0^2}, & \text{for } |\mathbf{v}| < v_{\text{esc}}, \\ 0, & \text{for } |\mathbf{v}| > v_{\text{esc}}, \end{cases} \quad (31)$$

where the maximum speed is equal to the galaxy escape velocity, v_{esc} , and

$$N = \pi^{3/2} v_0^3 \left[\text{erf}\left(\frac{v_{\text{esc}}}{v_0}\right) - \frac{2v_{\text{esc}}}{\sqrt{\pi}v_0} e^{-\left(\frac{v_{\text{esc}}}{v_0}\right)^2} \right]. \quad (32)$$

In this way, if \mathbf{v}_E is the velocity of the Earth with respect to the galactic frame, then⁹

$$f_{\oplus}(\mathbf{v}_{\text{rel}}) = f(\mathbf{v}_{\text{rel}} + \mathbf{v}_E). \quad (33)$$

For the numerical analysis we took the values used by the XENON1T Collaboration [80], namely, $v_0 = 220 \text{ km/s}$, $v_{\text{esc}} = 544 \text{ km/s}$, and $v_E = 232 \text{ km/s}$.

In the case of the direct detection experiment XENON1T, the number of expected events, $\mathcal{N}_{\text{events}}$, can be determined as [81]

⁹Given the functional dependence of $\frac{d\sigma_{\psi T}}{dE_R}$ with v_{rel} , the integrals

$$\zeta(E_R) = \int_{v_{\min}(E_R)}^{\infty} \frac{d^3 \mathbf{v}_{\text{rel}}}{v_{\text{rel}}} f(\mathbf{v}_{\text{rel}} + \mathbf{v}_E),$$

$$\xi(E_R) = \int_{v_{\min}(E_R)}^{\infty} d^3 \mathbf{v}_{\text{rel}} v_{\text{rel}} f(\mathbf{v}_{\text{rel}} + \mathbf{v}_E),$$

must be calculated when determining $\frac{dR}{dE_R}$. Analytical expressions for these integrals can be found in Appendix C of Ref. [74].

$$\mathcal{N}_{\text{events}} = \omega_{\text{exp}} \int_{S_{\min}}^{S_{\max}} dS \sum_{n=1}^{\infty} \text{Gauss}(S|n, \sqrt{n}\sigma_{\text{PMT}}) \times \int_0^{\infty} dE_R \epsilon(E_R) \text{Pois}(n|\nu(E_R)) \frac{dR}{dE_R}. \quad (34)$$

Here $\omega_{\text{exp}} = 278.8 \text{ days} \times 1.30 \text{ tons}$ is the exposure, $S \in [3, 70]$ is the number of photoelectrons (PE) resulting from the collision between the WIMP DM candidate and a Xe nucleus ($A = 131$, $Z = 54$, $m_T = 122.0 \text{ GeV}$); σ_{PMT} is the average single-PE resolution of the photomultipliers, $\epsilon(E_R)$ is the detection efficiency and $\nu(E_R)$ is the expected number of PEs for a given recoil energy E_R . For the numerical estimate of $\mathcal{N}_{\text{events}}$ we took $\sigma_{\text{PMT}} = 0.4$ [82,83], whereas $\epsilon(E_R)$ was extracted from the black solid line in Fig. 1 of Ref. [80]. $\nu(E_R)$, for its part, was calculated as

$$\nu(E_R) = E_R \mathcal{L}_{\text{eff}} \mathcal{L}_y S_{\text{NR}}, \quad (35)$$

where the average light yield \mathcal{L}_y was fixed in 7.7 PE/keV [84] and a value of 0.95 was assigned to the light yield suppression factor for nuclear recoils S_{NR} . The relative scintillation efficiency \mathcal{L}_{eff} was extracted from Fig. 1 in Ref. [85].

From the most recent data reported by XENON1T, and with the aid of a test statistic (TS), we can obtain an upper bound for $\mathcal{N}_{\text{events}}$. Closely following Ref. [86], we take

$$\text{TS}(m_\psi) = -2 \ln \left[\frac{\mathcal{L}(\mathcal{N}_{\text{events}})}{\mathcal{L}_{\text{BG}}} \right], \quad (36)$$

with

$$\mathcal{L}(\mathcal{N}_{\text{events}}) = \frac{(\mathcal{N}_{\text{events}} + \mathcal{N}_{\text{BG}})^{\mathcal{N}_{\text{obs}}}}{\mathcal{N}_{\text{obs}}!} e^{-(\mathcal{N}_{\text{events}} + \mathcal{N}_{\text{BG}})}, \quad (37)$$

and $\mathcal{L}_{\text{BG}} \equiv \mathcal{L}(0)$. It follows that by demanding the $\text{TS}(m_\psi) > 2.71$, limits for $\mathcal{N}_{\text{events}}$ are obtained at 90% C.L. For $\mathcal{N}_{\text{obs}} = 14$ (number of observed events) and $\mathcal{N}_{\text{BG}} = 7.36(61)$ (number of background events) [80], the expected number of events must fulfill $\mathcal{N}_{\text{events}} \lesssim 19.5$ [74].

IV. NUMERICAL RESULTS

In order to study the fermion DM phenomenology and take into account the constraints associated with charged LFV processes, we have implemented the model in SARAH [60,61] to calculate, via SPheno [62,63] and FlavorKit [64], the flavor observables. In addition, we have used micrOMEGAS [73] to calculate the ψ relic abundance. We have performed a random scan over the relevant free parameters of the model as shown in Table II and assumed $\lambda_2 = \lambda_\Phi = \lambda_{h\Phi} = \lambda_S = 0.01$. Moreover, the mass of the exotic quark, M_D , has been set to $\sim 10 \text{ TeV}$ along with $f_\beta = 0.1$ in order to avoid the LHC constraints (see below).

TABLE II. Random sampling for the relevant free parameters used in the numerical analysis.

$1 \text{ GeV} \leq m_{\psi_1} \leq 500 \text{ GeV}$
$2m_{\psi_1} \leq m_{\psi_2} \leq 1 \text{ TeV}$
$\max(1.5m_{\psi_1}, 70 \text{ GeV}) \leq m_{S_1} \leq 1 \text{ TeV}$
$m_{S_1} \leq m_{S_2} \leq 2 \text{ TeV}$
$-\pi/2 \leq \varphi \leq \pi/2$
$10^{-5} \leq h_{\beta j} \leq \sqrt{4\pi}$
$10^9 \text{ GeV} \leq v_S \leq 10^{13} \text{ GeV}$
$0 < \theta_a \leq 2\pi$

TABLE III. Current bounds and projected sensitivities for charged LFV observables.

Observable	Present limit	Future sensitivity
$\mathcal{B}(\mu \rightarrow e\gamma)$	5.3×10^{-13} [91]	6.3×10^{-14} [92]
$\mathcal{B}(\tau \rightarrow e\gamma)$	3.3×10^{-8} [93–95]	3×10^{-9} [96]
$\mathcal{B}(\tau \rightarrow \mu\gamma)$	4.4×10^{-8} [93–95]	3×10^{-9} [96]
$\mathcal{B}(\mu \rightarrow eee)$	1.0×10^{-12} [97]	10^{-16} [98]
$\mathcal{B}(\tau \rightarrow eee)$	4.4×10^{-8} [99]	3×10^{-9} [96]
$\mathcal{B}(\tau \rightarrow \mu\mu\mu)$	2.1×10^{-8} [99]	10^{-9} [96]
$R_{\mu e}(\text{Ti})$	4.3×10^{-12} [100]	10^{-18} [101]
$R_{\mu e}(\text{Au})$	7.3×10^{-13} [102]	–

Let us recall that the $y_{i\beta}$ Yukawa couplings are linked to neutrino masses and the PMNS mixing matrix elements through the $h_{\beta j}$ Yukawa couplings as shown in Sec. II. The Large Electron-Positron Collider II constraints [87,88] on the H^\pm charged scalar are automatically satisfied by the scan conditions defined in Table II and we also ensure that the oblique parameters S , T , and U remain at 3σ level [89].¹⁰ Concerning to the neutrino parameters, we consider both hierarchies for neutrino masses and use the best-fit point values reported in Ref. [90] for the \mathcal{CP} conserving case. Finally, regarding the charged LFV processes we consider the current experimental bounds and their future expectations as shown in Table III.

We have calculated the fermion DM one-loop scattering cross section and estimated the expected number of events in direct detection experiments, $\mathcal{N}_{\text{events}}$, following the procedure described in Sec. III. The results are shown in Figs. 4 and 5. In Fig. 4, we present $\mathcal{N}_{\text{events}}$ as a function of the scalar mixing angle ($|\sin\varphi|$). All the points satisfy the current LFV constraints and the current limit imposed by the XENON1T Collaboration. The prospect limits expected by XENONnT are indicated by the horizontal dashed line [80]. Notice that a large fraction of the parameter space (red points) will be explored in the coming years (those

¹⁰For simplicity purposes, we are taking $\lambda_3 = 0$ in such a way that the charged and neutral components of the scalar doublet are degenerate.

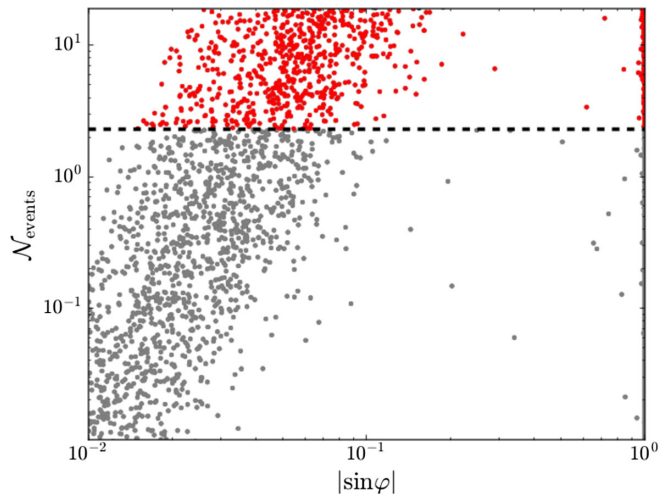


FIG. 4. Expected number of events as a function of the scalar mixing angle. All the points satisfy the current limit imposed XENON1T and the dashed line denotes the projected sensitivity of XENONnT experiment [80].

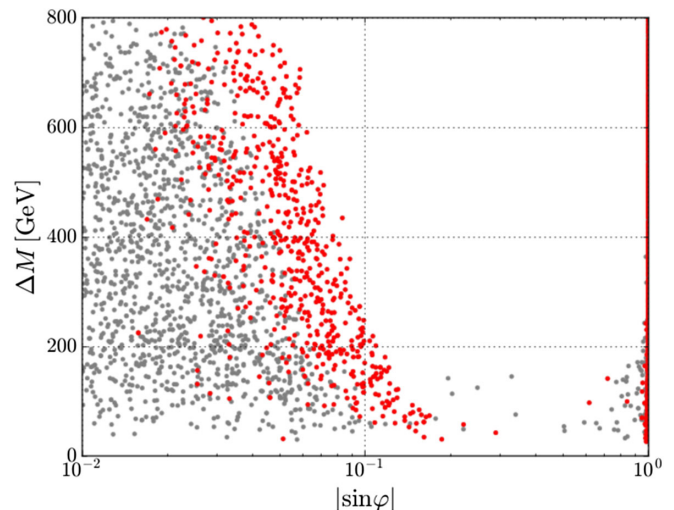


FIG. 5. The mass splitting $\Delta M \equiv m_{H^\pm} - m_\psi$ as a function of the scalar mixing angle. All the points satisfy the current limit imposed XENON1T and the red ones are those that will be explored by XENONnT.

featuring a small mixing angle are beyond the projected sensitivity, although such a small mixing angle is favored by the tiny neutrino masses). From Fig. 4 we also notice that for either $\varphi \rightarrow 0$ or $\varphi \rightarrow \pm\pi/2$, the number of events decreases rapidly, being steeper for $|\varphi| \rightarrow \pi/2$. This happens because when $\varphi \rightarrow 0$, the effective coupling between ψ and the Higgs ($C_{\psi h}$) becomes more suppressed than the case $|\varphi| \rightarrow \pi/2$ [see Eq. (26)]. However, the coupling between ψ and the Z boson ($C_{\psi Z}$) remains unaltered for both cases. Consequently, the expected number of events falls down more slowly for low small-mixing angles. On the other hand, when the mixing is appreciable the

contributions to $C_{\psi h}$ and $C_{\psi Z}$ coming from the neutral component of the scalar doublet H_2 become relevant, thus increasing the number of events in such a way it becomes maximum for $\varphi \sim \pi/4$.

In Fig. 5 we display the mass splitting $\Delta M \equiv m_{H^\pm} - m_\psi$ as a function of the scalar mixing angle. As in Fig. 4, the gray points are allowed by the current experimental searches, whereas the red ones represent the region that will be explored in the next years. Notice that in the case of maximal mixing ($|\varphi| \sim \pi/4$), where the number of events reaches its maximum value, there are some points localized in the allowed region. For these points the mass splitting between the charged scalar and ψ is small, $\Delta M \lesssim 50$ GeV, which means that the coannihilation processes are relevant. Conversely, for either $\varphi \rightarrow 0$ or $\varphi \rightarrow \pm\pi/2$ where the number of events drops sharply, the mass splitting can take any value in the allowed range determined in the scan.

We now discuss the axion phenomenology. The contribution of ψ to the total DM relic density $R_\psi = \Omega_\psi / (\Omega_\psi + \Omega_a)$ as a function of the axion mass is shown in Fig. 6. Each point reproduces the observed DM relic density $\Omega h^2 = 0.120 \pm 0.001$ at 3σ [103] and satisfies the direct detection constraints on ψ as well as the charged LFV bounds. The color code represents the corresponding axion-photon coupling, $g_{a\gamma} \sim \frac{\alpha}{2\pi v_S}$, which plays a main role in axion searches through helioscope and haloscope experiments [104–106]. For $v_S \lesssim 10^{10}$ GeV the main contribution to the DM relic abundance comes from the fermion DM candidate, with the corresponding axion mass window laying outside the experimental searches. However, for increasing values of v_S the mixed fermion-axion DM scenario becomes more relevant and the axion can account

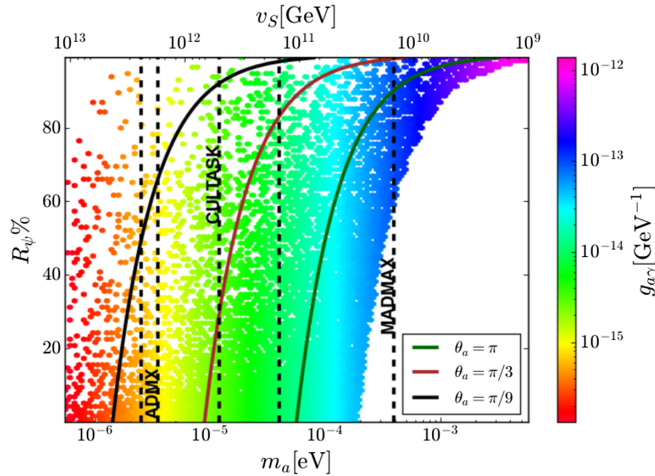


FIG. 6. ψ contribution to the total DM relic density as a function of the axion mass m_a and the axion-photon coupling, $g_{a\gamma} \sim \frac{\alpha}{2\pi v_S}$, for different values of the initial misalignment angle θ_a . The vertical dashed lines represent the regions that will be explored by the cavity haloscope experiments ADMX [108,109], CULTASK [110,111], and MADMAX [112–115].

for a fraction or the whole of the DM relic abundance. In this case, a large fraction of the axion mass window [with the axion-photon coupling taking values in the range $g_{a\gamma} \sim (5 \times 10^{-16} - 10^{-13})$ GeV $^{-1}$] can be explored by several haloscope experiments [105,106]; ADMX for $m_a \sim (2.5 - 3.5)$ μ eV, CULTASK for $m_a \sim (3.5 - 12)$ μ eV, and MADMAX for $m_a \sim (0.04 - 0.4)$ meV. Let us notice, however, that some regions are beyond the reach of the projected sensitivity of the experiments. Nonetheless, by enlarging the particle content or changing the PQ charge assignment on the current fields of the model, the chiral anomaly coefficient in the $g_{a\gamma}$ coupling can be modified in such a way that the entire region planned to search QCD axions in KSVZ and DFSZ models becomes experimentally accessible [105–107].

Regarding the charged LFV processes, we focus on the observables involving muons in the initial state. In Fig. 7 are displayed the branching ratios $\mathcal{B}(\mu \rightarrow e\gamma)$ (cyan points), $\mathcal{B}(\mu \rightarrow 3e)$ (magenta points), and the rate for the $\mu \rightarrow e$ conversion in titanium $\mathcal{R}_{\mu e}$ (blue points) as a function of the Yukawa coupling y_{21} . The left (right) panel stands for the normal (inverted) neutrino mass hierarchy, with the dotted, solid, and dashed horizontal lines representing the projected sensitivity of LFV experiments for $\mathcal{B}(\mu \rightarrow e\gamma)$, $\mathcal{B}(\mu \rightarrow 3e)$, and $\mathcal{R}_{\mu e}$, respectively. It follows that for both neutrino mass hierarchies the current bounds demand $|y_{21}| \lesssim 0.1$ whereas the future searches will explore values as low as 0.01, with the conversion in the nuclei being the most relevant process (we have found similar results for the other Yukawa couplings, $y_{i\beta}$). In addition to this, we notice that the observables associated with the lepton conversion in nuclei and the process with three electrons in the final state are strongly correlated. This is because the conversion process in nuclei does not involve box diagrams whereas the corresponding contribution in $\mu \rightarrow 3e$ becomes suppressed by a factor $|y_{i\beta}|^4$ and therefore the penguin diagrams give the dominant contribution for both charged LFV processes. This strong correlation, along with the correlation from $\mathcal{B}(\mu \rightarrow e\gamma)$, is shown in Fig. 8. On the other hand, we observed that the Yukawa couplings $h_{\beta i}$ can take values along the whole range considered in the scan. This result along with the ones for $y_{i\beta}$ discussed above translate to that the scalar coupling $|\lambda'|$ lies below 10^{-7} in order to reproduce the observed neutrino mass scale [see Eq. (9)].

A final comment is in order concerning the exotic quark D . Since it couples to the SM sector through the Yukawa term, $\overline{q}_L H_2 D_R$, it can decay into a $S_{1,2}$ scalar and a SM quark, thus avoiding potential issues that arise when an exotic quark is considered cosmologically stable [116]. Furthermore, such an exotic quark can be produced at colliders via quark and gluon fusion, leading to the specific signature of jets plus missing energy. From the analysis presented in Ref. [44], which deals with a scenario similar to the one

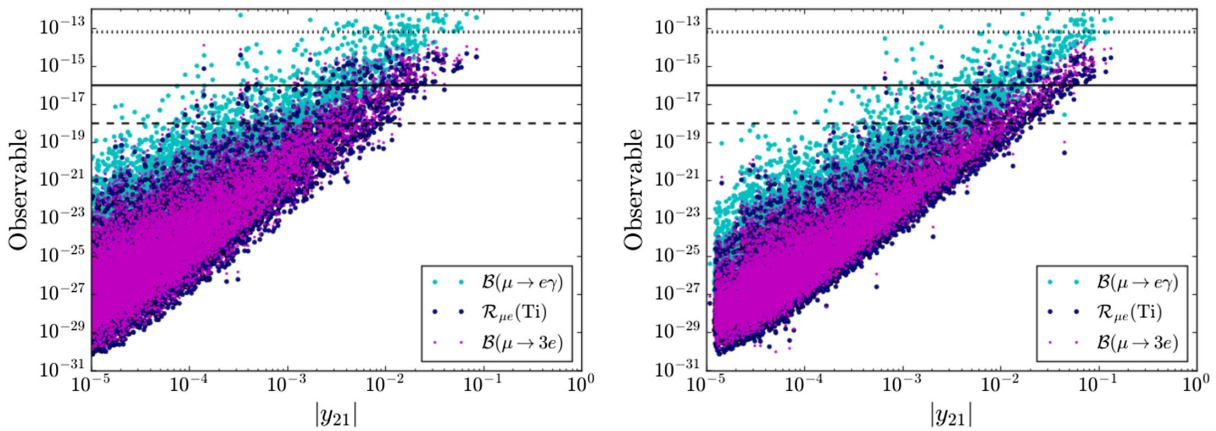


FIG. 7. Branching ratios for charged LFV processes involving muons as a function of $|y_{21}|$ for the normal (left) and inverted (right) neutrino-mass hierarchy.

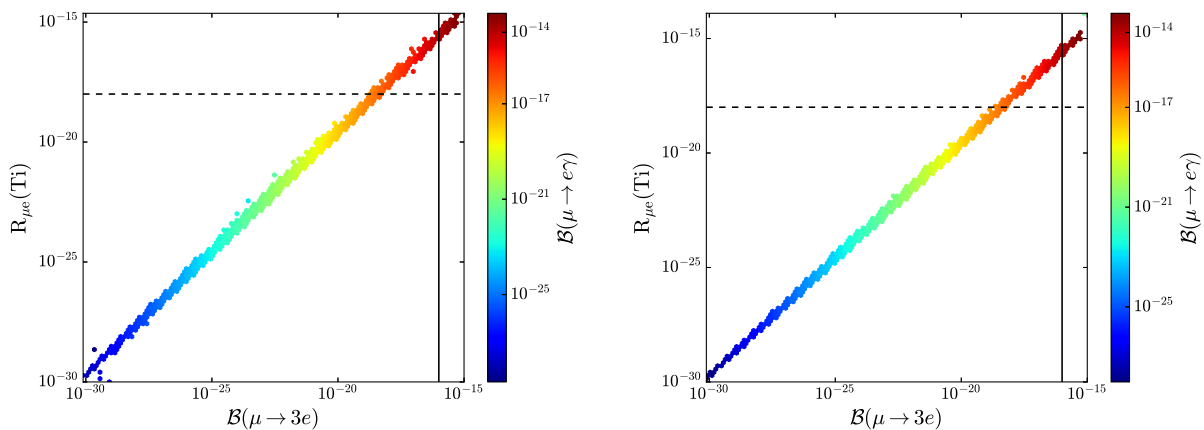


FIG. 8. Correlation between the different LFV observables involving muons. The left and right panels correspond to a IH and NH, respectively. The solid and dashed lines represent the expected sensitivity for the future searches $\mathcal{B}(\mu \rightarrow 3e)$ and $\mathcal{R}_{\mu e}$, respectively.

studied here, the LHC searches for exotic quarks imply that $M_D \gtrsim 700$ GeV, which is well below the value considered in our analysis.

V. CONCLUSIONS

In the class of models known as scotogenic models the generation of radiative neutrino masses is associated with the existence of a discrete symmetry that forbids the tree-level contribution and stabilizes the DM particle. Along these lines, the PQ symmetry can also be invoked to simultaneously provide a solution to the strong CP problem, radiatively induce neutrino masses, and stabilize the particles lying in the dark sector. In this work we considered a multicomponent scotogenic model with Dirac neutrinos where the dark sector is composed by the QCD axion and a SM singlet fermion; the latter stabilized by the PQ symmetry. We computed the expected number of fermion-DM nuclei scatterings in XENON1T and identified regions of the parameter space compatible with observed

DM abundance, direct searches of singlet fermion and axion DM, neutrino oscillation data and the upper bounds on charged LFV processes. Furthermore, we find that for some choices of parameters both the singlet fermion and the axion present detection rates which are within the expected sensitivity of XENONnT and haloscope experiments such as ADMX, CULTASK, and MADMAX, respectively, and that the LFV processes involving muons in the initial state may be probed in upcoming rare leptonic decay experiments.

ACKNOWLEDGMENTS

We are thankful to Diego Restrepo and Nicolás Bernal for enlightening discussions. This work has been supported by Sostenibilidad-UdeA and the UdeA/CODI Grants No. 2017-16286 and No. 2020-33177. C.D.R.C. and R.L. acknowledge the financial support given by COLCIENCIAS through the Doctoral Scholarships No. 727-2015 and No. 617-2013.

APPENDIX: ONE-LOOP FUNCTIONS FOR EFFECTIVE INTERACTIONS OF FERMION DM

In this section we reproduce the expressions for the one-loop functions required to calculate the C_M^γ , C_R^γ , $C_{\psi h}$, and $C_{\psi Z}$ effective couplings [74]. The functions associated with C_M^γ , C_R^γ , and $C_{\psi h}$ and are given by

$$g_{M1}(m_\psi, M, m) = 1 - \frac{M^2 - m^2}{2m_\psi^2} \ln\left(\frac{M^2}{m^2}\right) + \frac{\Delta + m_\psi^2(M^2 - m_\psi^2 + m^2)}{2m_\psi^2} L, \quad (\text{A1})$$

$$g_{R1}(m_\psi, M, m) = \frac{1}{12} \left[\frac{8(M^2 - m^2) + m_\psi^2}{m_\psi^2} \ln\left(\frac{M^2}{m^2}\right) - \frac{4}{\Delta} \{4\Delta + m_\psi^2(M^2 + 3m^2) - m_\psi^4\} \right. \\ \left. - \frac{L}{m_\psi^2 \Delta} \{8\Delta^2 + (9M^2 - 5m_\psi^2 + 7m^2)m_\psi^2 \Delta - 4m^2 m_\psi^4 (3M^2 - m_\psi^2 + m^2)\} \right], \quad (\text{A2})$$

whereas, the one associated with $C_{\psi h}$ reads

$$\tilde{g}_{h1}(m_\psi, M_i, M_j, m) = \frac{1}{2} + \frac{M_i^2 + M_j^2 - 2(m^2 + m_\psi^2)}{4m_\psi^2} \ln\left(\frac{m^2}{M_i M_j}\right) \\ - \frac{M_i^4 + M_j^4 - 2(M_i^2 + M_j^2)(m^2 + m_\psi^2) - 2(m_\psi^4 - m^4)}{4m_\psi^2(M_i^2 - M_j^2)} \ln\left(\frac{M_i}{M_j}\right) \\ + \frac{(M_i^2 - m^2 - m_\psi^2)\Delta_i L_i - (M_j^2 - m^2 - m_\psi^2)\Delta_j L_j}{4m_\psi^2(M_i^2 - M_j^2)}. \quad (\text{A3})$$

The computation of $C_{\psi Z}$ involves the functions

$$g_{Z1}(m_\psi, M, m_i, m_j) = -\frac{1}{2}\Delta_{\epsilon,\mu} + \frac{1}{2}\ln M + \frac{m_i^2 \ln m_i - m_j^2 \ln m_j}{2(m_i^2 - m_j^2)} + \frac{m_i^2 + m_j^2 - 2M^2 - m_\psi^2}{2m_\psi^2} \\ + \frac{\ln\left(\frac{M^2}{m_i m_j}\right)}{4m_\psi^4} [m_i^4 + m_j^4 - m_i^2 m_j^2 - 3M^2(m_i^2 + m_j^2 - M^2) - m_\psi^2(m_i^2 + m_j^2 + 2M^2)] \\ - \frac{\ln\left(\frac{m_i}{m_j}\right)}{4m_\psi^4(m_i^2 - m_j^2)} \{2m_\psi^6 - 6m_\psi^4 M^2 + m_\psi^2 [6M^4 - 2M^2(m_i^2 + m_j^2) - m_i^4 - m_j^4] \\ - 2M^6 + 3M^4(m_i^2 + m_j^2) - 3M^2(m_i^4 + m_j^4) + m_i^6 + m_j^6\} \\ + \frac{1}{4m_\psi^4(m_i^2 - m_j^2)} \{[(M^2 - m_i^2)^2 + (M^2 - m_\psi^2)^2 - M^4]\Delta_i L_i - [(M^2 - m_j^2)^2 + (M^2 - m_\psi^2)^2 - M^4]\Delta_j L_j\}, \quad (\text{A4})$$

$$g_{Z2}(m_\psi, M, m_i, m_j) = \frac{1}{2} \ln\left(\frac{M^2}{m_i m_j}\right) + \frac{\ln\left(\frac{m_i}{m_j}\right)}{2(m_i^2 - m_j^2)} (2M^2 - 2m_\psi^2 - m_i^2 - m_j^2) + \frac{\Delta_i L_i - \Delta_j L_j}{2(m_i^2 - m_j^2)}, \quad (\text{A5})$$

$$\begin{aligned}
\tilde{g}_{Z1}(m_\psi, M_i, M_j, m) &= \frac{1}{2} \Delta_{\epsilon, \mu} - \frac{1}{2} \ln m - \frac{M_i^2 \ln M_i - M_j^2 \ln M_j}{2(M_i^2 - M_j^2)} + \frac{M_i^2 + M_j^2 - 2m^2 + m_\psi^2}{2m_\psi^2} \\
&+ \frac{3m^2(m^2 - M_i^2 - M_j^2) - m_\psi^2(M_i^2 + M_j^2) + M_i^4 + M_j^4 + M_i^2 M_j^2}{4m_\psi^4} \ln \left(\frac{m^2}{M_i M_j} \right) \\
&- \frac{\ln \left(\frac{M_i}{M_j} \right)}{4m_\psi^4 (M_i^2 - M_j^2)} [M_i^6 + M_j^6 - (3m^2 + m_\psi^2)(M_i^4 + M_j^4) + 3m^4(M_i^2 + M_j^2) \\
&- 2(m^2 - m_\psi^2)^2(m^2 + m_\psi^2)] + \frac{1}{4m_\psi^4 (M_i^2 - M_j^2)} \{ [(M_i^2 - m^2)^2 - m_\psi^4] \Delta_i L_i - [(M_j^2 - m^2)^2 - m_\psi^4] \Delta_j L_j \},
\end{aligned} \tag{A6}$$

where

$$\begin{aligned}
\Delta(m_\psi, M, m) &= m_\psi^4 - 2m_\psi^2(M^2 + m^2) + (M^2 - m^2)^2 \\
&= m^4 - 2m^2(M^2 + m_\psi^2) + (M^2 - m_\psi^2)^2 \\
&= M^4 - 2M^2(m_\psi^2 + m^2) + (m_\psi^2 - m^2)^2,
\end{aligned} \tag{A7}$$

and¹¹

$$L(m_\psi, M, m) = \frac{1}{\sqrt{\Delta}} \ln \left(\frac{M^2 + m^2 - m_\psi^2 + \sqrt{\Delta}}{M^2 + m^2 - m_\psi^2 - \sqrt{\Delta}} \right). \tag{A8}$$

Additionally, Δ_i and L_i denote the quantities $\Delta(m_\psi, M_i, m)$ and $L(m_\psi, M_i, m)$, respectively, while $\Delta_{\epsilon, \mu}$ is a divergent constant term.

From these general expressions we deduce appropriated formulas for the limiting cases $m \rightarrow 0$, $M_i = M_j$ and $m_i = m_j$. In what follows, and when possible, the resulting expressions will be written in terms of the parameters $x \equiv \frac{m}{M}$, $y \equiv \frac{m_\psi}{M}$, and $\delta \equiv x^4 - 2x^2(1 + y^2) + (1 - y^2)^2$. Thus, for example,

$$g_{M1}(m_\psi, M, m) = 1 + \frac{1 - x^2}{y^2} \ln x + \frac{(1 - x^2)^2 - (1 + x^2)y^2}{2y^2 \sqrt{\delta}} \ln \left(\frac{1 + x^2 - y^2 + \sqrt{\delta}}{1 + x^2 - y^2 - \sqrt{\delta}} \right), \tag{A9}$$

$$\begin{aligned}
g_{R1}(m_\psi, M, m) &= -\frac{1}{6} \left[8 \frac{1 - x^2}{y^2} + 1 \right] \ln x - \frac{1}{3\delta} [4(1 - x^2)^2 - (7 + 5x^2)y^2 + 3y^4] \\
&- \frac{1}{12y^2 \delta^{3/2}} \ln \left(\frac{1 + x^2 - y^2 + \sqrt{\delta}}{1 + x^2 - y^2 - \sqrt{\delta}} \right) [8(1 - x^2)^4 - (1 - x^2)^2(23 + 25x^2)y^2 \\
&+ (25 - 2x^2 + 25x^4)y^4 - (13 + 11x^2)y^6 + 3y^8].
\end{aligned} \tag{A10}$$

For the case $M_i \neq M_j$ and $m = 0$ we obtain

$$\tilde{g}_{h1}(m_\psi, M_i, M_j, 0) = \frac{1}{2} + \frac{m_\psi^2}{M_i^2 - M_j^2} \ln \left(\frac{M_i}{M_j} \right) + \frac{(M_i^2 - m_\psi^2)^2 \ln \left(\frac{M_i^2 - m_\psi^2}{M_i^2} \right) - (M_j^2 - m_\psi^2)^2 \ln \left(\frac{M_j^2 - m_\psi^2}{M_j^2} \right)}{2m_\psi^2 (M_i^2 - M_j^2)}, \tag{A11}$$

¹¹This expression for L is valid provided that $\Delta > 0$, which is always true in our model.

$$\begin{aligned} \tilde{g}_{Z1}(m_\psi, M_i, M_j, 0) &= \frac{1}{2} \Delta_{\epsilon,\mu} + \frac{1}{2m_\psi^4(M_i^2 - M_j^2)} \left[(M_i^4 - m_\psi^4)(M_i^2 - m_\psi^2) \ln\left(\frac{M_i^2 - m_\psi^2}{M_i^2}\right) \right. \\ &\quad \left. - (M_j^4 - m_\psi^4)(M_j^2 - m_\psi^2) \ln\left(\frac{M_j^2 - m_\psi^2}{M_j^2}\right) \right] + \frac{M_i^2 + M_j^2 + m_\psi^2}{2m_\psi^2}, \end{aligned} \quad (\text{A12})$$

whereas for $M_i = M_j \equiv M$ and $m \neq 0$

$$\tilde{g}_{h1}(m_\psi, M, M, m) = 1 + \frac{1 - x^2 - y^2}{y^2} \ln x + \frac{x^4 - 2x^2 + (1 - y^2)^2}{2y^2\sqrt{\delta}} \ln\left(\frac{1 + x^2 - y^2 + \sqrt{\delta}}{1 + x^2 - y^2 - \sqrt{\delta}}\right), \quad (\text{A13})$$

$$\begin{aligned} \tilde{g}_{Z1}(m_\psi, M, M, m) &= \frac{1}{2} \Delta_{\epsilon,\mu} - \frac{1}{2} \ln(mM) + \frac{1}{4} + \frac{6 - 6x^2 - y^2}{4y^2} + \frac{3 - 2y^2 - 3x^2(2 - x^2)}{2y^4} \ln x \\ &\quad + \frac{1}{4y^4\sqrt{\delta}} \ln\left(\frac{1 + x^2 - y^2 + \sqrt{\delta}}{1 + x^2 - y^2 - \sqrt{\delta}}\right) [3(1 - x^2)^3 + (3x^4 + 2x^2 - 5)y^2 + (1 - x^2)y^4 + y^6], \end{aligned} \quad (\text{A14})$$

The case $M_i = M_j \equiv M$ and $m = 0$ leads to

$$\tilde{g}_{h1}(m_\psi, M, M, 0) = 1 + \frac{1 - y^2}{y^2} \ln(1 - y^2), \quad (\text{A15})$$

$$\tilde{g}_{Z1}(m_\psi, M, M, 0) = \frac{1}{2} \Delta_{\epsilon,\mu} - \ln M + \frac{1}{4} - \frac{y^2 - 6}{4y^2} + \frac{3 - 5y^2 + y^4 + y^6}{2y^4(1 - y^2)} \ln(1 - y^2), \quad (\text{A16})$$

and the case $m_i = m_j \equiv m \neq 0$ involves the limiting functions

$$\begin{aligned} g_{Z1}(m_\psi, M, m, m) &= -\frac{1}{2} \Delta_{\epsilon,\mu} + \frac{1}{2} \ln(mM) - \frac{1}{4} - \frac{x^4 + 3(1 - 2x^2) - 2y^2(1 + x^2)}{2y^4} \ln x \\ &\quad - \frac{3(1 - x^2)^3 - 5(1 - x^4)y^2 + (1 - 3x^2)y^4 + y^6}{4y^4\sqrt{\delta}} \ln\left(\frac{1 + x^2 - y^2 + \sqrt{\delta}}{1 + x^2 - y^2 - \sqrt{\delta}}\right) + \frac{6x^2 + y^2 - 6}{4y^2}, \end{aligned} \quad (\text{A17})$$

$$g_{Z2}(m_\psi, M, m, m) = -\ln x - \frac{1 - x^2 + y^2}{2\sqrt{\delta}} \ln\left(\frac{1 + x^2 - y^2 + \sqrt{\delta}}{1 + x^2 - y^2 - \sqrt{\delta}}\right). \quad (\text{A18})$$

Finally, the limiting functions appearing in the case $m_i = m_j \equiv m = 0$ fulfill

$$g_{Z1}(m_\psi, M, 0, 0) = -\tilde{g}_{Z1}(m_\psi, M, M, 0). \quad (\text{A19})$$

Notice that, from Eqs. (A14) and (A17)

$$g_{Z1}(m_\psi, M, m, m) + \tilde{g}_{Z1}(m_\psi, M, M, m) = \frac{(x^2 + y^2)}{x^{-2}y^4} \ln x + \frac{(1 - x^2 + y^2)}{2x^{-2}y^2\sqrt{\delta}} \ln\left(\frac{1 + x^2 - y^2 + \sqrt{\delta}}{1 + x^2 - y^2 - \sqrt{\delta}}\right). \quad (\text{A20})$$

- [1] R. D. Peccei and H. R. Quinn, *CP Conservation in the Presence of Instantons*, *Phys. Rev. Lett.* **38**, 1440 (1977).
- [2] S. Weinberg, *A New Light Boson?*, *Phys. Rev. Lett.* **40**, 223 (1978).
- [3] F. Wilczek, *Problem of Strong p and t Invariance in the Presence of Instantons*, *Phys. Rev. Lett.* **40**, 279 (1978).
- [4] P. Sikivie, *Axion cosmology*, *Lect. Notes Phys.* **741**, 19 (2008).
- [5] J. Preskill, M. B. Wise, and F. Wilczek, *Cosmology of the invisible axion*, *Phys. Lett.* **120B**, 127 (1983).
- [6] L. F. Abbott and P. Sikivie, *A cosmological bound on the invisible axion*, *Phys. Lett.* **120B**, 133 (1983).
- [7] M. Dine and W. Fischler, *The not so harmless axion*, *Phys. Lett.* **120B**, 137 (1983).
- [8] R. N. Mohapatra and G. Senjanovic, *The superlight axion and neutrino masses*, *Z. Phys. C* **17**, 53 (1983).
- [9] Q. Shafi and F. W. Stecker, *Implications of a Class of Grand Unified Theories for Large Scale Structure in the Universe*, *Phys. Rev. Lett.* **53**, 1292 (1984).
- [10] P. Langacker, R. D. Peccei, and T. Yanagida, *Invisible axions and light neutrinos: Are they connected?*, *Mod. Phys. Lett. A* **01**, 541 (1986).
- [11] M. Shin, *Light Neutrino Masses and Strong CP Problem*, *Phys. Rev. Lett.* **59**, 2515 (1987); **60**, 383(E) (1988).
- [12] X. G. He and R. R. Volkas, *Models Featuring Spontaneous CP Violation: An Invisible Axion and Light Neutrino Masses*, *Phys. Lett. B* **208**, 261 (1988); **218**, 508(E) (1989).
- [13] Z. G. Berezhiani and M. Yu. Khlopov, *Cosmology of spontaneously broken gauge family symmetry*, *Z. Phys. C* **49**, 73 (1991).
- [14] S. Bertolini and A. Santamaria, *The strong CP problem and the solar neutrino puzzle: Are they related?*, *Nucl. Phys.* **B357**, 222 (1991).
- [15] E. Ma, *Making neutrinos massive with an axion in supersymmetry*, *Phys. Lett. B* **514**, 330 (2001).
- [16] G. Servant, *Baryogenesis from Strong CP Violation and the QCD Axion*, *Phys. Rev. Lett.* **113**, 171803 (2014).
- [17] S. Ipek and T. M. P. Tait, *Early Cosmological Period of QCD Confinement*, *Phys. Rev. Lett.* **122**, 112001 (2019).
- [18] D. Croon, J. N. Howard, S. Ipek, and T. M. P. Tait, *QCD baryogenesis*, *Phys. Rev. D* **101**, 055042 (2020).
- [19] R. T. Co and K. Harigaya, *Axiogenesis*, *Phys. Rev. Lett.* **124**, 111602 (2020).
- [20] A. D. Linde, *Axions in inflationary cosmology*, *Phys. Lett. B* **259**, 38 (1991).
- [21] S. Folkerts, C. Germani, and J. Redondo, *Axion dark matter and Planck favor non-minimal couplings to gravity*, *Phys. Lett. B* **728**, 532 (2014).
- [22] M. Fairbairn, R. Hogan, and D. J. E. Marsh, *Unifying inflation and dark matter with the Peccei-Quinn field: Observable axions and observable tensors*, *Phys. Rev. D* **91**, 023509 (2015).
- [23] G. Ballesteros, J. Redondo, A. Ringwald, and C. Tamarit, *Unifying Inflation with the Axion, Dark Matter, Baryogenesis and the Seesaw Mechanism*, *Phys. Rev. Lett.* **118**, 071802 (2017).
- [24] C. D. R. Carvajal and Ó. Zapata, *One-loop Dirac neutrino mass and mixed axion-WIMP dark matter*, *Phys. Rev. D* **99**, 075009 (2019).
- [25] C.-S. Chen and L.-H. Tsai, *Peccei-Quinn symmetry as the origin of Dirac neutrino masses*, *Phys. Rev. D* **88**, 055015 (2013).
- [26] B. Dasgupta, E. Ma, and K. Tsumura, *Weakly interacting massive particle dark matter and radiative neutrino mass from Peccei-Quinn symmetry*, *Phys. Rev. D* **89**, 041702 (2014).
- [27] S. Bertolini, L. Di Luzio, H. Kolečová, and M. Malinský, *Massive neutrinos and invisible axion minimally connected*, *Phys. Rev. D* **91**, 055014 (2015).
- [28] P.-H. Gu, *Peccei-Quinn symmetry for Dirac seesaw and leptogenesis*, *J. Cosmol. Astropart. Phys.* **07** (2016) 004.
- [29] E. Ma, D. Restrepo, and Ó. Zapata, *Anomalous leptonic U(1) symmetry: Synthetic origin of the QCD axion, weak-scale dark matter, and radiative neutrino mass*, *Mod. Phys. Lett. A* **33**, 1850024 (2018).
- [30] E. Ma, T. Ohata, and K. Tsumura, *Majoron as the QCD axion in a radiative seesaw model*, *Phys. Rev. D* **96**, 075039 (2017).
- [31] D. Suematsu, *Dark matter stability and one-loop neutrino mass generation based on Peccei-Quinn symmetry*, *Eur. Phys. J. C* **78**, 33 (2018).
- [32] D. Suematsu, *Possible roles of Peccei-Quinn symmetry in an effective low energy model*, *Phys. Rev. D* **96**, 115004 (2017).
- [33] M. Reig, J. W. F. Valle, and F. Wilczek, *SO(3) family symmetry and axions*, *Phys. Rev. D* **98**, 095008 (2018).
- [34] M. Reig and R. Srivastava, *Spontaneous proton decay and the origin of Peccei-Quinn symmetry*, *Phys. Lett. B* **790**, 134 (2019).
- [35] E. Peinado, M. Reig, R. Srivastava, and J. W. F. Valle, *Dirac neutrinos from Peccei-Quinn symmetry: A fresh look at the axion*, *Mod. Phys. Lett. A* **35**, 2050176 (2020).
- [36] S. Baek, *Dirac neutrino from the breaking of Peccei-Quinn symmetry*, *Phys. Lett. B* **805**, 135415 (2020).
- [37] L. M. G. de la Vega, N. Nath, and E. Peinado, *Dirac neutrinos from Peccei-Quinn symmetry: Two examples*, *Nucl. Phys.* **B957**, 115099 (2020).
- [38] A. G. Dias, J. Leite, J. W. F. Valle, and C. A. Vaquera-Araujo, *Reloading the axion in a 3-3-1 setup*, *Phys. Lett. B* **810**, 135829 (2020).
- [39] S. Baek, *A connection between flavour anomaly, neutrino mass, and axion*, *J. High Energy Phys.* **10** (2020) 111.
- [40] E. Ma and O. Popov, *Pathways to naturally small Dirac neutrino masses*, *Phys. Lett. B* **764**, 142 (2017).
- [41] C.-Y. Yao and G.-J. Ding, *Systematic analysis of Dirac neutrino masses from a dimension five operator*, *Phys. Rev. D* **97**, 095042 (2018).
- [42] H. Baer, A. Lessa, S. Rajagopalan, and W. Sreethawong, *Mixed axion/neutralino cold dark matter in supersymmetric models*, *J. Cosmol. Astropart. Phys.* **06** (2011) 031.
- [43] K. J. Bae, H. Baer, and E. J. Chun, *Mixed axion/neutralino dark matter in the SUSY DFSZ axion model*, *J. Cosmol. Astropart. Phys.* **12** (2013) 028.
- [44] A. Alves, D. A. Camargo, A. G. Dias, R. Longas, C. C. Nishi, and F. S. Queiroz, *Collider and dark matter searches in the inert doublet model from Peccei-Quinn symmetry*, *J. High Energy Phys.* **10** (2016) 015.

- [45] S. Chatterjee, A. Das, T. Samui, and M. Sen, Mixed WIMP-axion dark matter, *Phys. Rev. D* **100**, 115050 (2019).
- [46] J.E. Kim, Weak Interaction Singlet and Strong CP Invariance, *Phys. Rev. Lett.* **43**, 103 (1979).
- [47] M. A. Shifman, A. I. Vainshtein, and V. I. Zakharov, Can confinement ensure natural CP invariance of strong interactions?, *Nucl. Phys.* **B166**, 493 (1980).
- [48] Y. Farzan and E. Ma, Dirac neutrino mass generation from dark matter, *Phys. Rev. D* **86**, 033007 (2012).
- [49] W. Wang and Z.-L. Han, Naturally small Dirac neutrino mass with intermediate $SU(2)_L$ multiplet fields, *J. High Energy Phys.* **04** (2017) 166.
- [50] D. Borah and A. Dasgupta, Common origin of neutrino mass, dark matter and Dirac leptogenesis, *J. Cosmol. Astropart. Phys.* **12** (2016) 034.
- [51] W. Wang, R. Wang, Z.-L. Han, and J.-Z. Han, The $B - L$ scotogenic models for Dirac neutrino masses, *Eur. Phys. J. C* **77**, 889 (2017).
- [52] C.-Y. Yao and Gui-Jun Ding, Systematic study of one-loop Dirac neutrino masses and viable dark matter candidates, *Phys. Rev. D* **96**, 095004 (2017).
- [53] E. Ma and U. Sarkar, Radiative left-right Dirac neutrino mass, *Phys. Lett. B* **776**, 54 (2018).
- [54] M. Reig, D. Restrepo, J.W.F. Valle, and O. Zapata, Bound-state dark matter and Dirac neutrino masses, *Phys. Rev. D* **97**, 115032 (2018).
- [55] J. Calle, D. Restrepo, C.E. Yaguna, and Ó. Zapata, Minimal radiative Dirac neutrino mass models, *Phys. Rev. D* **99**, 075008 (2019).
- [56] J. Calle, D. Restrepo, and Ó. Zapata, Dirac neutrino mass generation from a Majorana messenger, *Phys. Rev. D* **101**, 035004 (2020).
- [57] N. Bernal, J. Calle, and D. Restrepo, Anomaly-free Abelian gauge symmetries with Dirac scotogenic models, *Phys. Rev. D* **103**, 095032 (2021).
- [58] P. A. Zyla *et al.* (Particle Data Group), Review of particle physics, *Prog. Theor. Exp. Phys.* **2020**, 083C01 (2020).
- [59] E. Arganda and M. J. Herrero, Testing supersymmetry with lepton flavor violating τ and μ decays, *Phys. Rev. D* **73**, 055003 (2006).
- [60] F. Staub, SARAH 4: A tool for (not only SUSY) model builders, *Comput. Phys. Commun.* **185**, 1773 (2014).
- [61] F. Staub, Exploring new models in all detail with SARAH, *Adv. High Energy Phys.* **2015**, 840780 (2015).
- [62] W. Porod, SPheno, a program for calculating supersymmetric spectra, SUSY particle decays and SUSY particle production at $e + e-$ colliders, *Comput. Phys. Commun.* **153**, 275 (2003).
- [63] W. Porod and F. Staub, SPheno 3.1: Extensions including flavour, CP -phases and models beyond the MSSM, *Comput. Phys. Commun.* **183**, 2458 (2012).
- [64] W. Porod, F. Staub, and A. Vicente, A flavor kit for BSM models, *Eur. Phys. J. C* **74**, 2992 (2014).
- [65] G. Grilli di Cortona, E. Hardy, J. P. Vega, and G. Villadoro, The QCD axion, precisely, *J. High Energy Phys.* **01** (2016) 034.
- [66] L. Di Luzio, M. Giannotti, E. Nardi, and L. Visinelli, The landscape of QCD axion models, *Phys. Rep.* **870**, 1 (2020).
- [67] P. Arias, D. Cadamuro, M. Goodsell, J. Jaeckel, J. Redondo, and A. Ringwald, WISPy cold dark matter, *J. Cosmol. Astropart. Phys.* **06** (2012) 013.
- [68] R. L. Davis, Goldstone bosons in string models of galaxy formation, *Phys. Rev. D* **32**, 3172 (1985).
- [69] D. Harari and P. Sikivie, On the evolution of global strings in the early universe, *Phys. Lett. B* **195**, 361 (1987).
- [70] R. A. Battye and E. P. S. Shellard, Axion String Constraints, *Phys. Rev. Lett.* **73**, 2954 (1994); **76**, 2203(E) (1996).
- [71] T. Hiramatsu, M. Kawasaki, K. Saikawa, and T. Sekiguchi, Production of dark matter axions from collapse of string-wall systems, *Phys. Rev. D* **85**, 105020 (2012); **86**, 089902 (E) (2012).
- [72] K. J. Bae, J.-H. Huh, and J. E. Kim, Update of axion CDM energy, *J. Cosmol. Astropart. Phys.* **09** (2008) 005.
- [73] G. Belanger, F. Boudjema, A. Pukhov, and A. Semenov, micrOMEGAs_3: A program for calculating dark matter observables, *Comput. Phys. Commun.* **185**, 960 (2014).
- [74] J. Hisano, R. Nagai, and N. Nagata, Singlet Dirac fermion dark matter with mediators at loop, *J. High Energy Phys.* **12** (2018) 059.
- [75] J. Ellis, N. Nagata, and K. A. Olive, Uncertainties in WIMP dark matter scattering revisited, *Eur. Phys. J. C* **78**, 569 (2018).
- [76] M. A. Shifman, A. I. Vainshtein, and V. I. Zakharov, Remarks on higgs-boson interactions with nucleons, *Phys. Lett. B* **78**, 443 (1978).
- [77] J. D. Lewin and P. F. Smith, Review of mathematics, numerical factors, and corrections for dark matter experiments based on elastic nuclear recoil, *Astropart. Phys.* **6**, 87 (1996).
- [78] R. H. Helm, Inelastic and elastic scattering of 187-Mev electrons from selected even-even nuclei, *Phys. Rev.* **104**, 1466 (1956).
- [79] E. Aprile *et al.* (XENON Collaboration), First Dark Matter Search Results from the XENON1T Experiment, *Phys. Rev. Lett.* **119**, 181301 (2017).
- [80] E. Aprile *et al.* (XENON Collaboration), Dark Matter Search Results from a One Ton-Year Exposure of XENON1T, *Phys. Rev. Lett.* **121**, 111302 (2018).
- [81] E. Aprile *et al.* (XENON100 Collaboration), Likelihood approach to the first dark matter results from XENON100, *Phys. Rev. D* **84**, 052003 (2011).
- [82] E. Aprile *et al.* (XENON Collaboration), Lowering the radioactivity of the photomultiplier tubes for the XENON1T dark matter experiment, *Eur. Phys. J. C* **75**, 546 (2015).
- [83] P. Barrow *et al.*, Qualification tests of the R11410-21 photomultiplier tubes for the XENON1T detector, *J. Instrum.* **12**, P01024 (2017).
- [84] E. Aprile *et al.* (XENON Collaboration), Physics reach of the XENON1T dark matter experiment, *J. Cosmol. Astropart. Phys.* **04** (2016) 027.
- [85] E. Aprile *et al.* (XENON100 Collaboration), Dark Matter Results from 100 Live Days of XENON100 Data, *Phys. Rev. Lett.* **107**, 131302 (2011).
- [86] M. Cirelli, E. Del Nobile, and P. Panci, Tools for model-independent bounds in direct dark matter searches, *J. Cosmol. Astropart. Phys.* **10** (2013) 019.

- [87] P. Achard *et al.* (L3 Collaboration), Search for heavy neutral and charged leptons in e^+e^- annihilation at LEP, *Phys. Lett. B* **517**, 75 (2001).
- [88] E. Lundstrom, M. Gustafsson, and J. Edsjo, The inert doublet model and LEP II limits, *Phys. Rev. D* **79**, 035013 (2009).
- [89] M. Baak, J. Cúth, J. Haller, A. Hoecker, R. Kogler, K. Mönig, M. Schott, and J. Stelzer (Gfitter Group), The global electroweak fit at NNLO and prospects for the LHC and ILC, *Eur. Phys. J. C* **74**, 3046 (2014).
- [90] P. F. de Salas, D. V. Forero, C. A. Ternes, M. Tortola, and J. W. F. Valle, Status of neutrino oscillations 2018: 3σ hint for normal mass ordering and improved CP sensitivity, *Phys. Lett. B* **782**, 633 (2018).
- [91] J. Adam *et al.* (MEG Collaboration), New Constraint on the Existence of the $\mu^+ \rightarrow e^+\gamma$ Decay, *Phys. Rev. Lett.* **110**, 201801 (2013).
- [92] A. M. Baldini, F. Cei, C. Cerri, S. Dussoni, L. Galli *et al.*, MEG upgrade proposal, [arXiv:1301.7225](https://arxiv.org/abs/1301.7225).
- [93] B. Aubert *et al.* (BABAR Collaboration), Searches for Lepton Flavor Violation in the Decays $\tau^\pm \rightarrow e^\pm\gamma$ and $\tau^\pm \rightarrow \mu^\pm\gamma$, *Phys. Rev. Lett.* **104**, 021802 (2010).
- [94] M. Bona *et al.* (SuperB Collaboration), SuperB: A high-luminosity asymmetric e^+e^- super flavor factory. Conceptual design report, [arXiv:0709.0451](https://arxiv.org/abs/0709.0451).
- [95] Y. Miyazaki *et al.* (Belle Collaboration), Search for lepton-flavor-violating and lepton-number-violating $\tau \rightarrow \ell hh'$ decay modes, *Phys. Lett. B* **719**, 346 (2013).
- [96] T. Aushev *et al.*, Physics at super B factory, [arXiv:1002.5012](https://arxiv.org/abs/1002.5012).
- [97] U. Bellgardt *et al.* (SINDRUM Collaboration), Search for the decay $\mu^+ \rightarrow e^+e^+e^-$, *Nucl. Phys.* **B299**, 1 (1988).
- [98] A. Blondel, A. Bravar, M. Pohl, S. Bachmann, N. Berger *et al.*, Research proposal for an experiment to search for the decay $\mu \rightarrow eee$, [arXiv:1301.6113](https://arxiv.org/abs/1301.6113).
- [99] K. Hayasaka *et al.*, Search for lepton flavor violating τ decays into three leptons with 719 million produced $\tau^+\tau^-$ pairs, *Phys. Lett. B* **687**, 139 (2010).
- [100] C. Dohmen *et al.* (SINDRUM II Collaboration), Test of lepton flavor conservation in $\mu \rightarrow e$ conversion on titanium, *Phys. Lett. B* **317**, 631 (1993).
- [101] R. J. Abrams *et al.* (Mu2e Collaboration), Mu2e conceptual design report, [arXiv:1211.7019](https://arxiv.org/abs/1211.7019).
- [102] W. H. Bertl *et al.* (SINDRUM II Collaboration), A Search for muon to electron conversion in muonic gold, *Eur. Phys. J. C* **47**, 337 (2006).
- [103] N. Aghanim *et al.* (Planck Collaboration), Planck 2018 results. VI. Cosmological parameters, *Astron. Astrophys.* **641**, A6 (2020); **652**, C4(E) (2021).
- [104] P. Sikivie, Invisible axion search methods, *Rev. Mod. Phys.* **93**, 015004 (2021).
- [105] P. W. Graham, I. G. Irastorza, S. K. Lamoreaux, A. Lindner, and K. A. van Bibber, Experimental searches for the axion and axion-like particles, *Annu. Rev. Nucl. Part. Sci.* **65**, 485 (2015).
- [106] I. G. Irastorza and J. Redondo, New experimental approaches in the search for axion-like particles, *Prog. Part. Nucl. Phys.* **102**, 89 (2018).
- [107] L. Di Luzio, F. Mescia, and E. Nardi, Window for preferred axion models, *Phys. Rev. D* **96**, 075003 (2017).
- [108] N. Du *et al.* (ADMX Collaboration), A Search for Invisible Axion Dark Matter with the Axion Dark Matter Experiment, *Phys. Rev. Lett.* **120**, 151301 (2018).
- [109] T. Braine *et al.* (ADMX Collaboration), Extended Search for the Invisible Axion with the Axion Dark Matter Experiment, *Phys. Rev. Lett.* **124**, 101303 (2020).
- [110] Y. K. Semertzidis *et al.*, Axion dark matter research with IBS/CAPP, [arXiv:1910.11591](https://arxiv.org/abs/1910.11591).
- [111] W. Chung, CULTASK, axion experiment at CAPP in Korea, in *Proceedings of the 13th Patras Workshop on Axions, WIMPs and WISPs* (DESY, 2018), pp. 97–101, [10.3204/DESY-PROC-2017-02/woohyun_chung](https://arxiv.org/abs/10.3204/DESY-PROC-2017-02/woohyun_chung).
- [112] A. Caldwell, G. Dvali, B. Majorovits, A. Millar, G. Raffelt, J. Redondo, O. Reimann, F. Simon, and F. Steffen (MADMAX Working Group), Dielectric Haloscopes: A New Way to Detect Axion Dark Matter, *Phys. Rev. Lett.* **118**, 091801 (2017).
- [113] P. Brun *et al.* (MADMAX Collaboration), A new experimental approach to probe QCD axion dark matter in the mass range above $40 \mu\text{eV}$, *Eur. Phys. J. C* **79**, 186 (2019).
- [114] A. J. Millar, G. G. Raffelt, J. Redondo, and F. D. Steffen, Dielectric haloscopes to search for axion dark matter: Theoretical foundations, *J. Cosmol. Astropart. Phys.* **01** (2017) 061.
- [115] D. Horns, J. Jaeckel, A. Lindner, A. Lobanov, J. Redondo, and A. Ringwald, Searching for WISPy cold dark matter with a dish antenna, *J. Cosmol. Astropart. Phys.* **04** (2013) 016.
- [116] E. Nardi and E. Roulet, Are exotic stable quarks cosmologically allowed?. *Phys. Lett. B* **245**, 105 (1990).